Eksergi
Chemical Engineering Journal
Vol 22, No. 2. 2025

ISSN: 1410-394X
e-ISSN: 2460-8203

Fabrication and Characterization of Psf-TiO_2/GO Membranes for Photocatalytic Decomposition of Dyes in Batik Liquid Waste

Rosyida Nofiana Arofah, Yeni Rahmawati, Fadlilatul Taufany, Siti Nurkhamidah*

Department of Chemical Engineering, Faculty of Industrial and System Engineering, Institut Teknologi Sepuluh Nopember, Surabaya, 60111, Indonesia

Artikel history:

Submitted 5 Mei 2025
Revision 6 Juni 2025
Accepted 10 Juni 2025
Online 18 Juni 2025

ABSTRACT: One of the important processes in making batik cloth is dyeing which requires large amounts of water. Liquid waste from washing and rinsing batik cloth produces color from residual dye and can be the main source of water pollution. One method of removing dyes is the ultrafiltration process using Membrane Technology for photocatalytic decomposition. In this research, polysulfone (PSf) membrane uses addition of different TiO_2 compositions (1, 1.5, 2, 3, and 5 wt.%) and graphene oxide (GO) of 0.5 wt.% composition as photocatalyst. The photocatalyst can store energy therefore the photocatalytic process can be performed in a visible light environment. To identify the best composition of photocatalysts, photocatalytic performances were tested by the removal of methyl violet as dye along with characterization of the membranes for the morphological and physicochemical properties using FTIR, SEM, XRD, and DMA. The highest performance under visible light was shown by a membrane containing 5 wt.% TiO_2, which provided a permeate flux of 22.97 L m^{-2} h^{-1} and dye removal of up to 89.84%. The findings indicated that the PSf membrane matrix's stability and photocatalytic enhanced potential are driven by the cooperative interaction between TiO_2 and GO nanoparticles, which function as photocatalysts.

Keywords: Batik liquid waste; Membrane; Methyl violet; Photodecomposition; Ultrafiltration

1. Introduction

Batik is woven fabric adorned with diverse patterns. The art of batik production dates back to the 17th century, showcasing a long-standing cultural heritage and craftsmanship that has been preserved through generations and is regarded by both Malaysia and Indonesia as a global national heritage of the Malay people (Apriyani, 2018). Batik industry in Indonesia, including renowned centers like Pekalongan with approximately 2,608 business units, contributes significantly to the economy (Nurainun et al., 2008). However, the industry's reliance on synthetic dyes creates environmental challenges due to their complex structures, which resist natural decomposition (Istirokhatun et al., 2021). Batik production generates substantial liquid waste, with small businesses in Jogjakarta and Pekalongan producing 125 and 100 liters per kilogram of batik, respectively (Apriyani, 2018). Batik waste could contain a maximum of 4.6 mg/l Pb (II) copper and 0.724 mg/l Cd (II) (Nyamiati et al., 2024). This waste, laden with high concentrations of dyes and suspended solids, poses serious environmental threats, including interference with water photosynthesis, harm to aquatic life, and risks to human health if not properly treated (Istirokhatun et al., 2021; Zakaria et al., 2023).

Photocatalytic decomposition combined with membrane technology represents an innovative and sustainable approach to mitigating liquid batik waste by breaking down complex organic dyes into chemically safer compounds through light-activated catalytic reactions (Moslan et al., 2023). By enabling the selective separation of pollutants according to characteristics which includes size, molecular weight, and charge, membrane technology significantly improves photodegradation. It functions effectively at ambient to moderate pressures and temperatures (Chafidz et al., 2019; Nada Mustika Maisarah et al., 2024; Nurkhamidah et al., 2020). However, this approach requires photocatalyst integration into the polymer matrix. Polymeric membrane coupled with photocatalyst should improve pollutant degradation, enhance selectivity, and offer energy efficiency, cost-effectiveness, and self-cleaning capabilities (Zhang et al., 2024). Titanium Dioxide (TiO_2) is a widely employed photocatalyst because of its strong oxidative potential, chemical stability, non-toxicity, and anti-fouling qualities (Amelia, Shitopyta, et al., 2023; Ashley et al., 2022). TiO_2 also increases membrane hydrophilicity; however, its wide band gap of 3.2 eV necessitates activation by UV light, which comprises only 5% of visible light (Kite et al., 2021; Nada et al., 2022; Nurkhamidah et al., 2018). Polysulfone (PSf) is common

* Corresponding author
Email address: nurkhamidah@its.ac.id

polymer materials widely utilized in dye filtration owing to its superior permeability, mechanical strength, and solute removal. However, its practical implementation is hindered by membrane fouling and low photocatalytic efficiency, demanding careful optimization with photocatalytic additives and to enhance performance in wastewater treatment applications (Zhang et al., 2024). While membrane incorporated with TiO_2 are widely used for dye decomposition, their reliance on UV, which poses challenges, limits their practical efficiency (Kusworo et al., 2023). In this context, the incorporation of graphene oxide (GO) may provide structural and functional advantages. GO serves as an efficient energy storage material, ascribed to its features of expansive surface area combined with superior thermal and chemical stability. This enables the photocatalytic process to persist even in the absence of UV light, allowing membranes embedded with GO to maintain their functionality even in dark conditions (Moslan et al., 2023). Consequently, the presence of carboxyl and hydroxyl groups within GO benefits as nanofillers since it increases hydrophilicity and porosity by raising the membrane surface's affinity for water, which enhances flow and rejection efficiency (Djoko Kusworo et al., 2023; Nurkhamidah et al., 2020; Nyamiati et al., 2021).

This study aims to fabricate an ultrafiltration membrane through nonsolvent induced phase separation technique, with polysulfone (PSf) serving as the polymer matrix. To enhance the membrane's performance, TiO_2 was incorporated into the dope solution at varying weight ratios, while graphene oxide (GO) was introduced at a fixed weight ratio. It is expected that GO inclusion and optimal TiO_2 loading will improve hydrophilicity, mechanical strength, and dye removal under visible light. The modified PSf-TiO_2/GO membranes, along with the unmodified pure PSf membrane were tested for its dye removal performance and underwent comprehensive characterization using multiple analytical methods: FTIR spectroscopy to assess chemical composition, XRD for crystalline structure evaluation, DMA to measure mechanical behaviour, and SEM imaging for microstructural examination.

2. Materials and Methods

2.1. Materials

Technical grade polysulfone (PSf) formed the base polymer matrix. The solvent system employed high-purity N-Methyl-2-pyrrolidone (NMP, ≥99.5% by GC analysis, sourced from Supelco). Two nanoscale additives were integrated: anatase titanium dioxide particles (mean diameter <25 nm, purity 99.7%) and multilayer graphene oxide (15-20 sheet thickness, edge oxidation 4-10%) Both nanomaterials were procured from Sigma-Aldrich. The phase inversion process utilized purified water (demineralized) as the precipitation medium. All chemical compounds were applied without undergoing supplementary purification procedures.

2.2. Methods

2.2.1. Membrane Preparation

Membranes were fabricated in the form of flat sheets membranes. The fabrication process is divided into two parts.

Dope Solution Preparation

To prevent the clustering of nanoparticles during the synthesis of the dope solution, the polymer solutions and nanoparticle suspensions were prepared individually. The membrane fabrication process began with the preparation of a PSf-based dope solution, where the polymer was completely dissolved in organic NMP solvent under continuous agitation for a duration of 4 hours to ensure complete dissolution and achieve a homogeneous mixture. This method was critical in maintaining uniform dispersion and optimizing the membrane's structural properties. GO and TiO_2 were dispersed in NMP in separate container and sonicated for 30 minutes. The compositions of each fabricated membrane were tabulated in Table 1 with TiO_2 concentration ranging from 0-5 wt.%, considering the agglomeration tendency of the particles upon higher concentration. Subsequently, the suspension of nanoparticles and the polymer solution were put together and agitated for 8 hours at room temperature. To get rid of any trapped air bubbles, the homogenous solution was left at rest for 4 hours at room temperature.

Phase Separation Process

In the flat sheet membrane casting process, the membrane was formed using a glass plate with a certain thickness and casted employing the technique of phase inversion. The polymer solution after casting was submerged carefully at a certain angle in a nonsolvent bath containing purified water to instigate phase separation and left at room temperature for 30 minutes. This process step was crucial for effecting the desired phase inversions, enabling the solidification of the membrane structure and ensuring proper pore formation for effective ultrafiltration performance. Following the fabrication process, the membrane was dried under ambient conditions.

2.2.2. Membrane Performance Test

Membrane performance was evaluated through dye rejection, filtration flux, and pure water flux using a custom filtration set-up simulating batik wastewater condition. These parameters provided a comprehensive assessment of the membrane's capability to filter dye pollutants, maintain consistent flow rates during filtration, and facilitate water permeability under controlled conditions. Figure 1 displays the schematic of the filtering apparatus. The filtering apparatus is a laboratory-scale crossflow equipment including a permeate tank, membrane cell housed within a sealed cell with a functional membrane exposure area of 12.57 cm^2, a diaphragm pump, a valve, and a pressure indicator. A solution with a 2-ppm concentration of methyl violet dye was employed as a model pollutant in the filtration

ISSN: 1410-394X
e-ISSN: 2460-8203

experiments. This setup was specifically chosen to simulate real-world dye contamination scenarios.

Flux determination was employed for pure water and filtration. The membrane's flux of pure water at 0.5 bar pressure was measured using demineralized water. The water flux was continuously measured by collecting the permeate solution for certain time intervals until a stable value of the pure water flux was achieved. The filtration flux of the membrane was evaluated using a methyl violet solution, applied under identical conditions to those used for measuring pure water flux, including the same operational pressure. Equation 1 was used to determine flux.

$$J_w = \frac{W}{A \cdot \Delta t} \quad (1)$$

Here, parameter J_w quantifies the permeate flux expressed in liters per square meter per hour (L m^{-2} h^{-1}), W denotes the total liquid volume in liters that permeated the membrane throughout the testing period (L), A refers to active separation surface measured in square meters (m^2), and Δt signifies the time interval in hours (h) over which the permeate is collected.

Methyl violet solution passing over the membrane was used to quantify the dye removal efficiency, and the permeate solution concentration was quantified via N4S UV-Vis spectrophotometer and identified with calibration curve from standard solution. Dye removal efficiency was calculated using Equation 2.

$$\%R = \left(1 - \frac{C_p}{C_f}\right) \times 100\% \quad (2)$$

In this equation, R represents the dye removal efficiency, expressed as a percentage (%) and dye concentration measurements are denoted as C_p for permeate output and C_f for feed input, both in mg/L (Meng et al., 2022; Yang et al., 2020).

Table 1. Dope Solution Composition

Samples	PSf (wt.%)	NMP (wt.%)	GO (wt.% PSf)	TiO_2 (wt.% PSf)
PSf	16	84	0	0
PSf-1	16	84	0.5	1
PSf-1.5	16	84	0.5	1.5
PSf-2	16	84	0.5	2
PSf-3	16	84	0.5	3
PSf-5	16	84	0.5	5

2.2.3. Membrane Characterization

Membrane surface morphology and membrane pore diameter were measured using a scanning electron microscope (SEM). Cryo-fracture techniques utilizing liquid nitrogen were applied to the membranes to preserve their structural integrity and then carefully placed on a sample stage for further analysis. This preparation method ensured minimal distortion, allowing for accurate characterization of the membrane's morphology and internal structure. Measurement of pore diameters was conducted via surface and cross-sectional morphological assessment. X-Ray Diffraction (XRD) analysis was conducted to identify and confirm the crystalline phase of the TiO_2 incorporated within the fabricated membrane, ensuring proper structural characterization. Additionally, hydroxyl group (–OH) on the membrane surface was characterized through Fourier-Transform Infrared Spectroscopic (FTIR) analysis, providing essential information about its chemical composition and surface functionalization. The mechanical characteristics of the membrane were evaluated by Dynamic Mechanical Analysis (DMA).

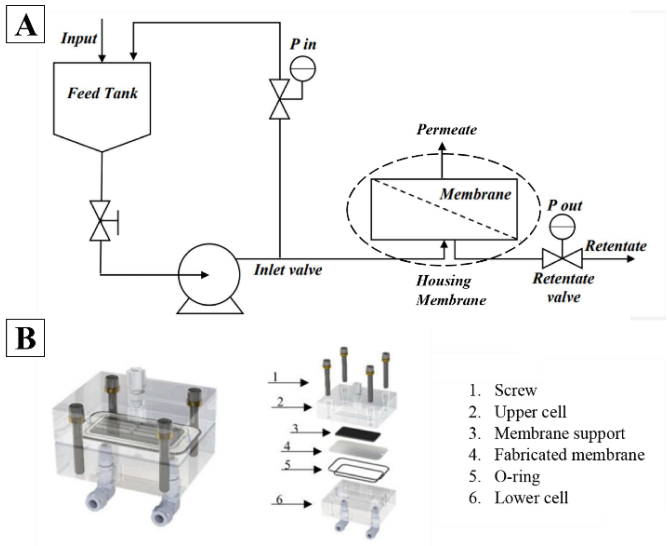

Figure 1. Schematic of Membrane Filtration Equipment. (a) Overall scheme; (b) Housing membrane details.

3. Results and Discussion

3.1. Membrane FTIR Spectra

Infrared absorption spectra were acquired for the modified and pure PSf membranes to assess their characteristics. Figure 2 presents the FTIR spectra for both the pure PSf membrane and the PSf-TiO_2/GO composite membranes, which were tested with increasing concentrations of TiO_2. Pure PSf membrane shows a broad peak at 3401 cm^{-1} as stretching vibration mode of hydroxyl groups (OH) which shows that there is water molecules present because of surface humidity or moisture absorption (Momeni & Pakizeh, 2013). All membranes exhibit absorption peaks corresponding to the PSf structure. Infrared spectral analysis shows a distinct absorption band centered at a wavelength of 2960 cm^{-1}, which is the characteristic of C-H stretching vibrations. Additionally, the significant absorption observed at 1149 cm^{-1} confirms the existence of the O=S=O bond, indicative of the vibrational bonding within the PSf matrix. Peaks at 1487 cm^{-1} and 1584 cm^{-1} are attributed to the aromatic C=C vibrational stretch, characteristic of the aromatic rings in the polysulfone structure. The absorption bands at 1295 cm^{-1} and 1323 cm^{-1} correspond to the vibrational modes of the S=O bond in the polysulfone group.

The characteristic C-H stretching vibration of aromatic rings appears at 2960 cm^{-1}. Lastly, the peak observed at 1239 cm^{-1} corresponds to C-O-C ether group stretching in the polysulfone backbone (Nasirian et al., 2020).

The TiO_2 incorporated in the membrane spectrum shows absorption peak at 691 cm^{-1}, indicating the Ti-O vibration, which typically appear within the standard range of 400–1000 cm^{-1} (Steephen et al., n.d.). The presence of C-O bonds is shown by absorption peaks for the graphene oxide spectra at 1105 cm^{-1} and 1149 cm^{-1} (Brusko et al., 2024). A spectral feature at 1585 cm^{-1} which is the characteristic of the bending vibration of C-OH groups, indicating the presence of hydroxyl functionality. Additionally, the absorption peak at 1684 cm^{-1} represents C=O stretching in graphene oxide's carboxyl groups, verifying its presence in the composite. These spectral features demonstrate the functional groups within the hybrid material (Sudesh et al., 2013).

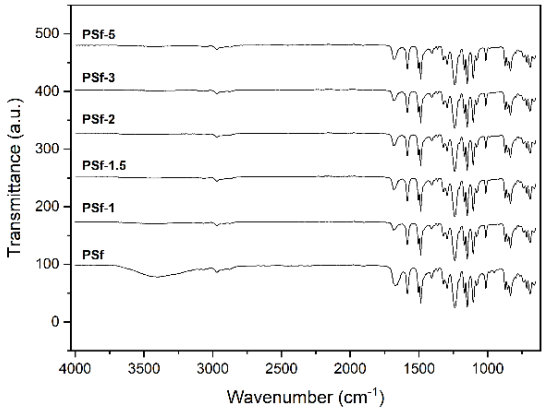

Figure 2. Fourier Transform Infrared Spectra (FTIR) of Pure PSf and PSf-TiO_2/GO Membranes

3.2. Membrane Morphological Characteristics

The morphological structure of the PES membranes fabricated and the distribution of TiO_2 particles were analyzed using Scanning Electron Microscope (SEM). Figure 3 showcases the membranes surface morphology that were developed for this research. It was revealed that the top surface's active skin layer had a thick, nanoporous structure. The pure PSf membrane had the most visible pore indicating larger pores compared to the modified membranes. The small pores in the modified membranes are formed by the filling of membrane pores due to the entrapment of inorganic TiO_2 particles, which can lead to reduced flux. The TiO_2 particles were distinctly identified as small white particles visible on the surface of the modified membranes, providing clear evidence of their incorporation into the membrane structure. These white particles were observable and helped confirm the existence of titania particles embedded in the membrane (Rahimpour et al., 2011). An evenly dispersed TiO_2 particles pattern is observed on the membrane surface, some of which group together to form bigger aggregates.

The cross-section of the membranes developed for this research is displayed in Figure 4. The membranes were subjected to freeze-fracturing while immersed in liquid nitrogen to prepare for cross-sectional views. Each membrane was produced via phase inversion technique, resulting in an asymmetric structure. This structure features a distinct porous sublayer, which resembles a finger-like pattern, and a dense, smooth top skin layer, contributing to the overall membrane morphology. In the cross-section area, a more developed finger-like structure can be observed with the introduction of TiO_2 and GO additive. The finger-like macrovoids appear slightly elongated and more regular with the increase of TiO_2 concentration. Besides that, the upper layer was thinner with the increase of TiO_2 concentration. This suggests that TiO_2 particles help in stabilizing the pore formation during membrane fabrication, possibly enhancing porosity (Kusworo et al., 2020). Membrane morphology is influenced by the amount of additive incorporated which is attributed to the enhanced hydrophilicity caused by varying concentrations of particle (Jaleh et al., 2020).

During the immersion precipitation process, the diffusional interactions of solvent and nonsolvent that drive polymer demixing during membrane production demonstrates a positive correlation with increasing particle amount in the polymer solution. This accelerated exchange promotes the formation of a more porous membrane and more defined macrovoid structures. The increased particle concentration accelerates the phase separation process, facilitating the development of a membrane with higher pore density and increased void fraction (Birsan et al., 2021). This indicates that high nanoparticle content can lead to excessive pore clogging, leading to a denser, more compact structure, which might reduce permeability but enhance mechanical strength and antifouling capability. The dimensions of membrane pores are directly correlated with the dynamics of solvent–nonsolvent exchange occurring throughout the phase separation step. When the displacement velocity is higher, larger holes tend to form, creating a more porous structure. On the other hand, a slower displacement velocity leads to smaller cavities or even a lack of cavities altogether, resulting in a denser membrane. These structural variations significantly influence the membrane's performance, including its efficiency, permeability, and flow rate, as the distribution of pores affects how substances pass through the material. The dynamics of phase inversion, particularly the rate at which polymer solution separates into distinct phases, fundamentally governs both the resulting pore architecture and membrane transport characteristics.

3.3. Membrane Mechanical Properties

Dynamic Mechanical Analysis (DMA) was utilized to thoroughly assess the mechanical performance exhibited by the membranes, with particular emphasis on assessing mechanical properties, specifically tensile strength and elongation-at-break percentages, yielding valuable information about the membrane's mechanical resilience and deformation resistance. Useful information on the membranes' resistance to tensile stress and elastic deformation during filtration processes was obtained by a thorough analysis of mechanical strength variables like

ISSN: 1410-394X
e-ISSN: 2460-8203

tensile strength (MPa) and elongation (%) at breaking point. Figure 5 presents representative stress-strain curves for both pure PSf membranes and the PSf-TiO_2/GO composite membranes. These curves provide a comparative analysis of the mechanical behavior of the two membrane types. As the TiO_2 concentration gets higher, the figure shows that the membrane's tensile strength generally enhances as well. Membrane with highest tensile strength was obtained by addition of 5 wt.% TiO_2 that reached 2.34 MPa, while membrane with lowest tensile strength was obtained by pure PSf membrane with the value of 1.55 MPa. Incorporation of TiO_2 enhanced the tensile strength due to the dispersed particles that was present in the membrane matrix helped enduring the applied force during mechanical testing (Kusworo et al., 2020). Other than TiO_2 particles, incorporation of GO assisted in resisting the energy applied to the membrane as well. Additionally, improved force load of the membrane resulted from the interactions between the particle and the polymer where the particles function as a bridging agent, increasing the interchain interaction and enhancing its durability (Sundaran et al., 2020; Yanilmaz et al., 2017).

However, it can be observed that the PSf-3 membrane broke first, suggesting the smallest breaking strength due to the stiffness of the material that cannot withstand elastic distortion. While PSf-2 membrane was the last one to break, indicating the maximum fracture strength.

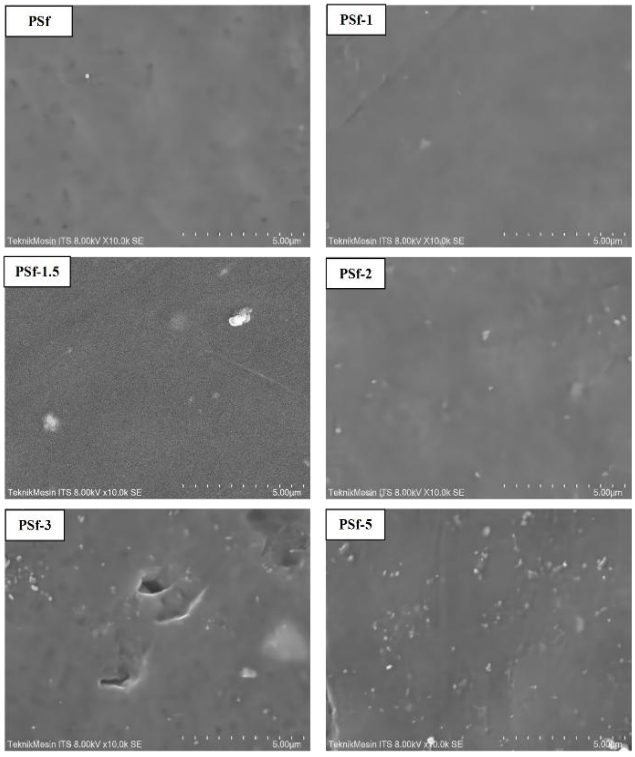

Figure 3. Scanning Electron Microscope (SEM) Image of Surface of Pure PSf and PSf-TiO_2/GO Membranes with Magnification of 10K

3.4. Membrane X-Ray Diffraction Patterns

Phase determination of the crystalline content is accomplished using X-Ray Diffraction (XRD) analysis. The pure PSf and PSf-TiO_2/GO membranes' XRD patterns are displayed in Figure 6. Every membrane displayed a large peak at $2\theta = 17.97°$, which corresponds to the polysulfone, in the 10° to 30° range. For PSf, this broad peak denotes an amorphous structure devoid of long-range crystalline structure (Badrinezhad et al., 2018).

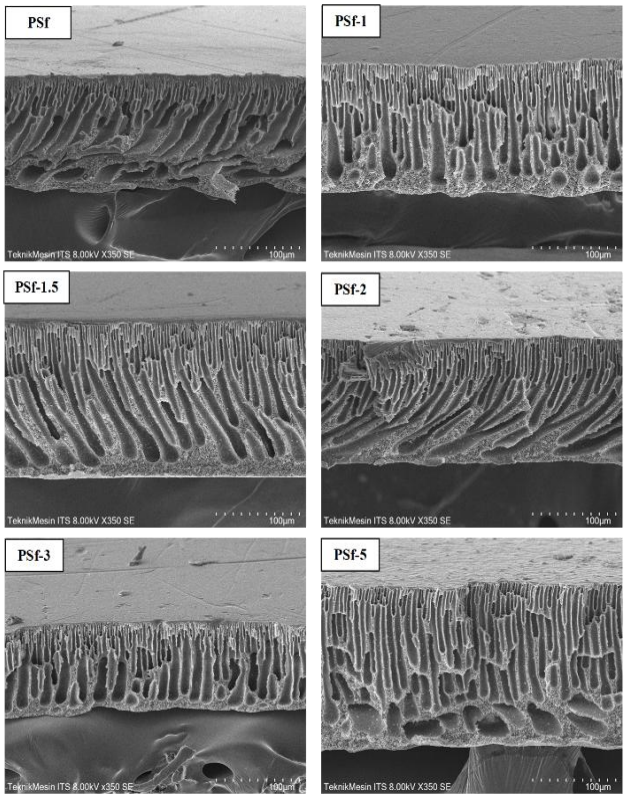

Figure 4. Scanning Electron Microscope (SEM) Image of Cross-Sectional Area of Pure PSf and PSf-TiO_2/GO Membranes with Magnification of 350

Other than pure PSf membrane, all the modified membranes showed a second peak at around 25° with varied sharpness. This peak is assigned to TiO_2 in the anatase form representing the refection of (101) planes (JCPDS 21-1272) (Li et al., 2014; Sundaran et al., 2020). The intensity and definition of spectral peaks vary with titania content. The higher the concentration, the sharpness of the of the peak increases as well. The sharpest peak of TiO_2 is obtained by incorporating 5 wt.% of TiO_2 into the matrix which gave the highest degree of crystallinity at 2θ values of 25.29°. Incorporating 5 wt.% of TiO_2 resulted in another peak at 2θ values of 48.04° which corresponds to TiO_2 anatase (200) crystal plane (Li et al., 2014).

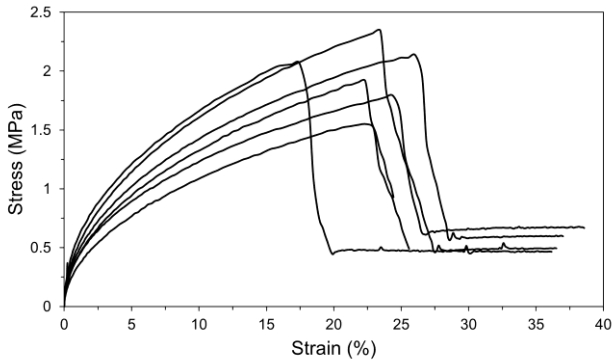

Figure 5. Stress-Strain Curve of Pure PSf and PSf-TiO_2/GO Membranes; TS: Tensile Strength

3.5. Pure Water Flux and Filtration Flux Evaluation

PSf as the polymer in membrane fabrication is a hydrophobic material which can cause intense membrane fouling due to the tendency of interacting with organic materials in its matrix (Fu et al., 2017). To enhance the hydrophilicity, incorporation of TiO_2 and GO is used. Because of the many hydrogen bonds that exist between water and the hydroxyl groups on its surface, TiO_2 has a high affinity for water (Zhang et al., 2022). Furthermore, the incorporation of GO greatly enhanced the membrane's water-attracting properties, increasing its hydrophilicity, yet also promoting the formation of larger macrovoids within the membrane structure. This alteration in the morphology contributed to a substantial enhancement in the permeate flux, facilitating improved filtration performance (Kusworo et al., 2021).

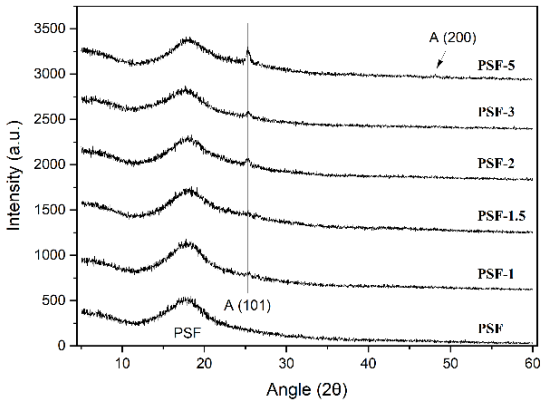

Figure 6. X-Ray Diffraction (XRD) Pattern for Pure PSf and PSf-TiO_2/GO Membranes

Figure 7 and Figure 8a show pure water flux and filtration flux of PSf-TiO_2/GO membrane with varied TiO_2 concentrations, respectively. The membrane's water flux was evaluated in a dead-end configuration employing demineralized water.

Simultaneously, the filtration performance was assessed employing methyl violet dye as a representative contaminant. Generally, the pure water flux has higher flux compared to the filtration flux. This happened because the dye started to clog the membrane pore during filtration. Overall results show that increasing TiO_2 concentrations improved the flux. Increasing the TiO_2 enhanced the hydrophilicity that renders it more feasible for water molecules to cross the membrane and inhibits hydrophobic interaction between membrane surface and organic foulant such as dyes (Jaleh et al., 2020; Sotto et al., 2011).

However, both results show that the highest flux was obtained by addition of 3 wt.% TiO_2. At higher concentration, the TiO_2 particles will excessively plug the membrane pores and decrease the flux. Apart from that, higher concentration of TiO_2 will lead to agglomeration of the particles due to the prominent surface energy (Zhang et al., 2022). Particles agglomeration results in defects on the membranes and is detrimental to the material properties (Mamah et al., 2021; Tian et al., 2022). Increase of particle size also leads to defective entrapment of the particle to the polymer matrix (Sotto et al., 2011).

3.6. Dye Removal Efficiency

A common mechanism for particle rejection in water treatment is based on the particle size. Upon rejecting the larger particles, Solutes with a size smaller than the membrane pores pass through the pores (Mamah et al., 2021).

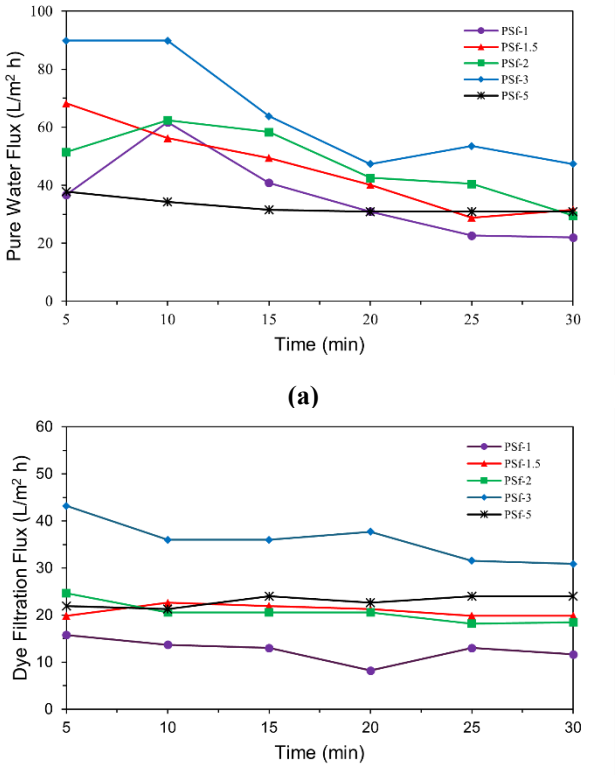

Figure 8. Effect of TiO_2 Concentration on (a) Pure Water Flux and (b) Dye Filtration Flux

ISSN: 1410-394X
e-ISSN: 2460-8203

A solution with 2 ppm concentration of methyl violet dye was utilized in the membrane filtering performance. Figure 8b. shows the rejection percentage of methyl violet as the model pollutant with varied TiO_2 concentrations. The highest methyl violet was achieved by addition of 5 wt.% of TiO_2 with the value of 89.84%. When TiO_2 particles were incorporated to the dope solution with increasing concentration, the rejection percentage increased. The inclusion of TiO_2 in the dope solution is responsible for this outcome, resulting in membranes exhibiting narrower pore size distributions at the top surface. The presence of TiO_2 influences the membrane's microstructure, resulting in a denser surface layer with reduced pore dimensions (Birsan et al., 2021; Rahimpour et al., 2011). Narrower surface pores will effectively retain the dye particles and allow the cleaner water to pass through.

Due to its limited UV photon flux, TiO_2 photocatalysis can only treat wastewaters with modest levels of pollutants, which is one of its drawbacks (Bet-Moushoul et al., 2016). To overcome this drawback, addition of GO can help degrading the dye even without UV exposure. GO is an excellent material for energy storage due to its considerably enormous surface area, allowing the capability of enhancing electrochemical charge storage and increased capacity to absorb light. The high surface area of GO facilitates greater interaction with charged species, making it an ideal candidate for applications in energy storage systems (Moslan et al., 2023).

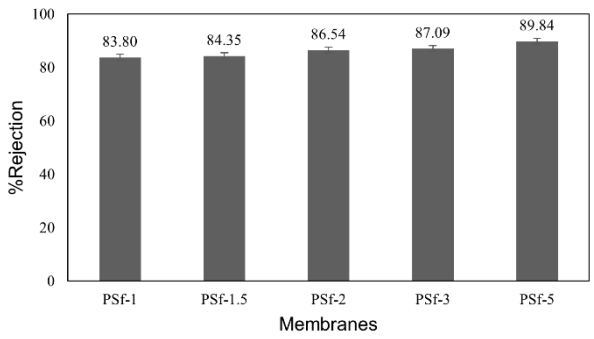

Figure 9. Effect of TiO_2 Concentration on Dye Removal

Functional groups in GO, such as –OH and –COOH, can form hydrogen bonds with nitrogen-containing functional groups in methyl violet, facilitating adsorption of methyl violet into the membrane matrix (Nastiti et al., 2020). Other than that, noting its role as an electron reservoir that can store and transport photo-excited electrons, the electron-hole recombination in TiO_2 can be reduced, extending TiO_2's photo-response to visible light, thus enhance photocatalytic activity (Minella et al., 2017). Under visible light, GO and TiO_2 generate reactive oxygen species like •OH and O_2•$^-$ that degrade methyl violet (Amelia, Jamilatun, et al., 2023). The surface of titania has hydroxyl groups that can act as electron donors in the formation of H^+. Therefore, the number of hydroxyl radicals that can degrade organic compound is increased (Heltina et al., 2020). Hydroxyl radicals (•OH) exhibit exceptional reactivity toward organic contaminants. Upon generation typically via photocatalytic activation, they initiate non-selective oxidative attacks on dye molecules such as methyl violet. As a result, the original dye is progressively transformed into a series of lower-molecular-weight intermediates and oxidative degradation products that are much safer (Ramesh et al., 2024). Figure 10 represents the schematic diagram of the photocatalytic reaction.

The optimum PSf-TiO_2/GO membrane achieved an impressive 89.84% rejection of methyl violet. While direct comparative studies employing this exact PSf-TiO_2/GO membrane configuration for methyl violet are limited, this rejection rate demonstrates excellent performance when compared to other membrane systems reported for similar materials and cationic dyes (Figure 9). Prior study utilizing the same polymer but loaded with TiO_2 and urea-assisted GO achieved methylene blue removal efficiencies of 77.5% under visible light (Xu et al., 2018).

Even though the highest flux was achieved by addition of 3 wt.% TiO_2, the highest rejection percentage was achieved with the highest addition of TiO_2. In membranes, rejection and flux must be balanced. Increasing the flux by creating larger pores in the membrane tends to decrease the rejection percentage since more pollutant particles will pass through (Kotobuki et al., 2021).

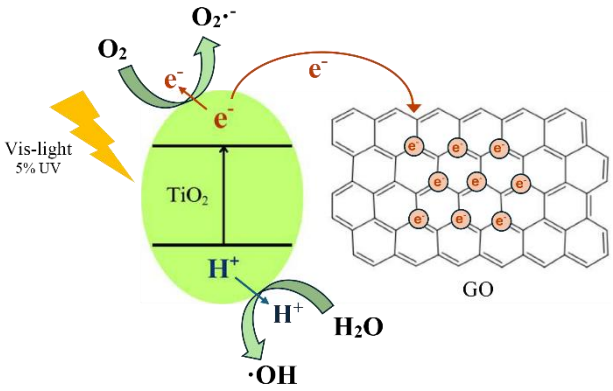

Figure 10. Schematic Diagram of Photocatalytic Reaction

While PSf-TiO_2/GO membranes demonstrated promising rejection results, it is crucial to critically examine the observed trade-offs inherent in composite membrane design. To potentially resolve this inherent trade-off and further enhance membrane performance, future research could explore more sophisticated membrane architectures. For instance, a dual-layer membrane design could be investigated. The first layer, potentially with a higher TiO_2 and GO loading, could be optimized for robust photocatalytic degradation and adsorption, while a second, thinner selective layer could prioritize high rejection and permeability. For the scaled real-world use of PSf-TiO_2/GO membranes in dye-concentrated wastewater treatment, the criteria for optimal performance would necessarily involve a

multi-faceted balance of several critical parameters such as long-term fouling and regeneration, rather than prioritizing maximum rejection or highest flux in isolation.

4. Conclusions

PSf-TiO_2/GO membranes were successfully synthesized with varying concentrations of TiO_2. The integration of TiO_2 and GO into the PSf membrane structure has shown considerable promise in enhancing both photocatalytic activity and filtration efficiency, particularly for the treatment of liquid batik waste. This composite membrane system exhibits improved performance in addressing the challenges associated with wastewater treatment, offering a more effective solution for pollutant removal. The SEM images of membranes showed fingerlike macrovoids with more developed pores with an increase in TiO_2. The study revealed that increasing TiO_2 concentration enhances hydrophilicity, mechanical strength, and dye rejection efficiency, with GO contributing to improved energy storage and enhanced porosity. However, excessive TiO_2 concentrations can lead to particle agglomeration and pore clogging, reducing flux. The membrane with 5 wt.% TiO_2 content exhibited the most favorable balance between permeate flux and rejection performance under visible light. It achieved a permeate flux of 22.97 L m^{-2} h^{-1}, coupled with a dye removal efficiency of up to 89.84%. These findings emphasize the importance of optimizing nanoparticle concentrations to balance permeability and rejection in photocatalytic membrane applications. Future research should focus on addressing UV light dependence and scaling up membrane fabrication for industrial applications.

Acknowledgements
This research has been funded by Kementerian Pendidikan, Kebudayaan, Riset, dan Teknologi 2024 with a contract number of 1851/PKS/ITS/2024.

Statement
During the preparation of this work the authors used ChatGPT 4.0 and Quilbot to improve English language and proofread the text. After using this tool/service, the authors reviewed and edited the content as needed and take full responsibility for the content of the publication.

CRediT authorship contribution statement
Rosyida Nofiana Arofah: Writing –review & editing, Writing – original draft, Visualization, Investigation, Formal analysis.
Siti Nurkhamidah: Validation, Resources, Conceptualization, Supervision.
Yeni Rahmawati: Validation, Resources, Conceptualization, Supervision.
Fadlilatul Taufany: Validation, Resources, Conceptualization.

Declaration of competing interest
The authors declare that they have no known competing financial interests or personal relationships that could have appeared to influence the work reported in this paper.

Data availability
The data that has been used is confidential.

References

Amelia, S., Jamilatun, S., Shitopyta, L. M., Maryudi, M., W, M. U., & Sriyana, I. (2023). Degradasi Limbah Detergen dengan Metode Fotokatalis Menggunakan TiO2 / Silica Gel. *Eksergi*, *20*(3), 131–136. https://doi.org/10.31315/E.V20I3.9214

Amelia, S., Shitopyta, L. M., W, M. U., & Sriyana, I. (2023). Color Degradation of Napthol Jeans with TiO2-SiO2 Photocatalyst from Karangwuni Beach Sand, Kulon Progo. *Eksergi*, *20*(1), 15–20. https://doi.org/10.31315/E.V20I1.8990

Apriyani, N. (2018). Industri Batik: Kandungan Limbah Cair dan Metode Pengolahannya. *MITL Media Ilmiah Teknik Lingkungan*, *3*(1), 21–29.

Ashley, A., Thrope, B., Choudhury, M. R., & Pinto, A. H. (2022). Emerging investigator series: Photocatalytic membrane reactors: Fundamentals and advances in preparation and application in wastewater treatment. *Environmental Science: Water Research and Technology*, *8*, 22–46. https://doi.org/10.1039/d1ew00513h

Badrinezhad, L., Ghasemi, S., Azizian-Kalandaragh, Y., & Nematollahzadeh, A. (2018). Preparation and characterization of polysulfone/graphene oxide nanocomposite membranes for the separation of methylene blue from water. *Polymer Bulletin*, *75*(2), 469–484. https://doi.org/10.1007/s00289-017-2046-7

Bet-Moushoul, E., Mansourpanah, Y., Farhadi, K., & Tabatabaei, M. (2016). TiO2 nanocomposite based polymeric membranes: A review on performance improvement for various applications in chemical engineering processes. *Chemical Engineering Journal*, 283, 29–46. https://doi.org/10.1016/j.cej.2015.06.124

Birsan, I. G., Pintilie, S. C., Pintilie, L. G., Lazar, A. L., Circiumaru, A., & Balta, S. (2021). New understanding of the difference in filtration performance between anatase and rutile tio2 nanoparticles through blending into ultrafiltration psf membranes. *Membranes*, *11*(11). https://doi.org/10.3390/membranes11110841

Brusko, V., Khannanov, A., Rakhmatullin, A., & Dimiev, A. M. (2024). Unraveling the infrared spectrum of graphene oxide. *Carbon*, *229*. https://doi.org/10.1016/j.carbon.2024.119507

Chafidz, A., Rahma, F. N., Nurkhamidah, S., & Al-Zahrani, S. (2019). Portable Solar-powered Membrane Distillation System to Solve Water and Energy

ISSN: 1410-394X
e-ISSN: 2460-8203

Problems Simultaneously. *Journal of Physics: Conference Series*, *1304*(1). https://doi.org/10.1088/1742-6596/1304/1/012018

Djoko Kusworo, T., Azizah, D. A., & Kumoro, A. C. (2023). Performance and Antifouling Evaluation of PSf/GO Nanohybrid Membrane on Removing Dye Pollutant from Batik Wastewater. *Waste Technology*, *11*(1), 17–27. https://doi.org/10.14710/wastech.11.1.17-27

Fu, W., Hua, L., & Zhang, W. (2017). Experimental and Modeling Assessment of the Roles of Hydrophobicity and Zeta Potential in Chemically Modified Poly(ether sulfone) Membrane Fouling Kinetics. *Industrial and Engineering Chemistry Research*, *56*(30), 8580–8589. https://doi.org/10.1021/acs.iecr.7b02203

Heltina, D., Putri, N. G., Panca, D., & Utama, S. (2020). Effect of the Phenol Concentration on the Phenol Photodegradation Effectivity using TitaniaCarbon Nanotube-cocoPAS Composite. *Eksergi*, *17*(2), 39–44. https://doi.org/10.31315/E.V17I2.3691

Istirokhatun, T., Susanto, H., Budihardjo, M. A., Septiyani, E., Wibowo, A. R., & Karamah, E. F. (2021). Treatment of Batik Industry Wastewater Plant Effluent using Nanofiltration. *International Journal of Technology*, *12*(4), 770–780. https://doi.org/10.14716/ijtech.v12i4.4645

Jaleh, B., Zare, E., Azizian, S., Qanati, O., Nasrollahzadeh, M., & Varma, R. S. (2020). Preparation and Characterization of Polyvinylpyrrolidone/Polysulfone Ultrafiltration Membrane Modified by Graphene Oxide and Titanium Dioxide for Enhancing Hydrophilicity and Antifouling Properties. *Journal of Inorganic and Organometallic Polymers and Materials*, *30*(6), 2213–2223. https://doi.org/10.1007/s10904-019-01367-x

Kite, S. V., Kadam, A. N., Sathe, D. J., Patil, S., Mali, S. S., Hong, C. K., Lee, S. W., & Garadkar, K. M. (2021). Nanostructured TiO2Sensitized with MoS2Nanoflowers for Enhanced Photodegradation Efficiency toward Methyl Orange. *ACS Omega*, *6*(26), 17071–17085. https://doi.org/10.1021/acsomega.1c02194

Kotobuki, M., Gu, Q., Zhang, L., & Wang, J. (2021). Ceramic-Polymer Composite Membranes for Water and Wastewater Treatment: Bridging the Big Gap between Ceramics and Polymers. *Molecules*, *26*(11). https://doi.org/https://doi.org/10.3390/molecules26113331

Kusworo, T. D., Ariyanti, N., & Utomo, D. P. (2020). Effect of nano-TiO2 loading in polysulfone membranes on the removal of pollutant following natural-rubber wastewater treatment. *Journal of Water Process Engineering*, *35*. https://doi.org/10.1016/j.jwpe.2020.101190

Kusworo, T. D., Kumoro, A. C., & Yulfarida, M. (2023). A new visible-light driven photocatalytic PVDF-MoS2@WO3 membrane for clean water recovery from natural rubber wastewater. *Journal of Water Process Engineering*, *52*, 103522. https://doi.org/10.1016/j.jwpe.2023.103522

Kusworo, T. D., Susanto, H., Aryanti, N., Rokhati, N., Widiasa, I. N., Al-Aziz, H., Utomo, D. P., Masithoh, D., & Kumoro, A. C. (2021). Preparation and characterization of photocatalytic PSf-TiO2/GO nanohybrid membrane for the degradation of organic contaminants in natural rubber wastewater. *Journal of Environmental Chemical Engineering*, *9*(2). https://doi.org/10.1016/j.jece.2021.105066

Li, W., Liang, R., Hu, A., Huang, Z., & Zhou, Y. N. (2014). Generation of oxygen vacancies in visible light activated one-dimensional iodine TiO2 photocatalysts. *RSC Advances*, *4*(70), 36959–36966. https://doi.org/10.1039/c4ra04768k

Mamah, S. C., Goh, P. S., Ismail, A. F., Suzaimi, N. D., Yogarathinam, L. T., Raji, Y. O., & El-badawy, T. H. (2021). Recent development in modification of polysulfone membrane for water treatment application. *Journal of Water Process Engineering*, 40 https://doi.org/10.1016/j.jwpe.2020.101835

Meng, N., Zhu, X., & Lian, F. (2022). Particles in composite polymer electrolyte for solid-state lithium batteries: A review. *Particuology*, *60*, 14–36. https://doi.org/10.1016/J.PARTIC.2021.04.002

Minella, M., Sordello, F., & Minero, C. (2017). Photocatalytic process in TiO2/graphene hybrid materials. Evidence of charge separation by electron transfer from reduced graphene oxide to TiO2. *Catalysis Today*, *281*, 29–37. https://doi.org/10.1016/J.CATTOD.2016.03.040

Momeni, S. M., & Pakizeh, M. (2013). Preparation, characterization and gas permeation study of psf/mgo nanocomposite membrane. *Brazilian Journal of Chemical Engineering*, *30*(3), 589–597. https://doi.org/10.1590/S0104-66322013000300016

Moslan, M. S., Othman, M. H. D., Zakria, H. S., Ismail, N. J., Borhamdin, S., Rahman, M. A., Jaafar, J., Puteh, M. H., Hashim, N., Kerisnan, N. D. A. P., Yahaya, N. K. E. M., & Idris, A. (2023). Photocatalytic degradation of bisphenol A and energy storage capability of novel MoO3/ZnO/GO under visible light irradiation. *Journal of Materials Science*, *58*(22), 9233–9250. https://doi.org/10.1007/s10853-023-08580-7

Nada, E. A., El-Maghrabi, H. H., Raynaud, P., Ali, H. R., El-Wahab, S. A., Sabry, D. Y., Moustafa, Y. M., & Nada, A. A. (2022). Enhanced Photocatalytic Activity of WS2/TiO2 Nanofibers for Degradation of Phenol under Visible Light Irradiation. *Inorganics*, *10*(4). https://doi.org/10.3390/inorganics10040054

Maisarah, N. M., Nurkhamidah, S., Altway, A., Susianto, Taufany, F., Cahyo, Z. A. I., Sari, D. P., & Rahmawati, Y. (2024). The Comparison of Polyethersulfone (PES)/N-Methyl 2-Pyrrolidone (NMP) on the Fabrication of Hollow Fiber Membranes with Commercial Membranes for Applications

Hemodialysis. *Materials Science Forum*, 43–50. https://doi.org/doi.org/10.4028/p-h8YUss

Nasirian, D., Salahshoori, I., Sadeghi, M., Rashidi, N., & Hassanzadeganroudsari, M. (2020). Investigation of the gas permeability properties from polysulfone/polyethylene glycol composite membrane. *Polymer Bulletin*, *77*(10), 5529–5552. https://doi.org/10.1007/s00289-019-03031-3

Nastiti, E. P., Hidayati, N., & Yani, J. A. (2020). Preparation and Characterization of sPEEK-PVA Composite Membranes with Graphene Oxide as filler for Direct Methanol Fuel Cells. *Eksergi*, *17*(2), 68–72. https://doi.org/10.31315/E.V17I2.3729

Nurainun, Heriyana, & Rasyimah. (2008). ANALISIS INDUSTRI BATIK DI INDONESIA. *Fokus Ekonomi (FE)*, *7*(3), 124–135.

Nurkhamidah, S., Devi, B. C., Febriansyah, B. A., Ramadhani, A., Nyamiati, R. D., Rahmawati, Y., & Chafidz, A. (2020). Characteristics of Cellulose Acetate/Polyethylene Glycol membrane with the addition of Graphene Oxide by using surface coating method. *IOP Conference Series: Materials Science and Engineering*, *732*(1). https://doi.org/10.1088/1757-899X/732/1/012002

Nurkhamidah, S., Rahmawati, Y., Gunardi, I., Alifiyanti, P., Dimas Priambodo, K., Luthfi Zaim, R., & Eka Muqni, W. (2018). Enhancing Properties and Performance of Cellulose Acetate/Polyethylene Glycol (CA/PEG) Membrane with the addition of Titanium Dioxide (TiO2) by Using Surface Coating Method. *MATEC Web of Conferences*, *156*. https://doi.org/10.1051/matecconf/201815608016

Nyamiati, R. D., Devi, B. C., Febriansyah, B. A., Ramadhani, A., Rahmawati, Y., & Nurkhamidah, S. (2021). Effect of Graphene Oxide on the Performance of Cellulose Acetate/ Polyethylene Glycol Membrane with Blending Method for Desalination of Brackish Water. *IOP Conference Series: Materials Science and Engineering*, *1143*(1), 012059. https://doi.org/10.1088/1757-899x/1143/1/012059

Nyamiati, R. D., Timotius, D., Rahmawati, S. S. S., Carissavila, C., & Amalia, N. (2024). Effect of Chitosan-TiO2 Membrane Performance for the Degradation of Batik Waste with a Photocatalytic Hybrid System. *Eksergi*, *21*(1), 44–47. https://doi.org/10.31315/E.V21I1.10734

Rahimpour, A., Jahanshahi, M., Rajaeian, B., & Rahimnejad, M. (2011). TiO2 entrapped nano-composite PVDF/SPES membranes: Preparation, characterization, antifouling and antibacterial properties. *Desalination*, *278*(1–3), 343–353. https://doi.org/10.1016/j.desal.2011.05.049

Ramesh, N., Lai, C. W., Johan, M. R. Bin, Mousavi, S. M., Badruddin, I. A., Kumar, A., Sharma, G., & Gapsari, F. (2024). Progress in photocatalytic degradation of industrial organic dye by utilising the silver doped titanium dioxide nanocomposite. *Heliyon*, *10*(24), e40998. https://doi.org/10.1016/J.HELIYON.2024.E40998

Sotto, A., Boromand, A., Zhang, R., Luis, P.,Arsuaga, J. M., Kim, J., & Van der Bruggen, B. (2011). Effect of nanoparticle aggregation at low concentrations of TiO 2 on the hydrophilicity, morphology, and fouling resistance of PES-TiO 2 membranes. *Journal of Colloid and Interface Science*, *363*(2), 540–550. https://doi.org/10.1016/j.jcis.2011.07.089

Steephen, A., Murugakoothan, P., Ananth, S., Vivek, P., & Arumanayagam, T. (2013). Natural Dye Extracts of Areca Catechu Nut as dye Sensitizer for Titanium dioxide Based Dye Sensitized Solar Cells. *J. Nano-Electron. Phys,* *6*(1), 01003-1 - 01003-4. https://www.researchgate.net/publication/263238658

Sudesh, Kumar, N., Das, S., Bernhard, C., & Varma, G. D. (2013). Effect of graphene oxide doping on superconducting properties of bulk MgB2. *Superconductor Science and Technology*, *26*(9). https://doi.org/10.1088/0953-2048/26/9/095008

Sundaran, S. P., Reshmi, C. R., Sagitha, P., & Sujith, A. (2020). Polyurethane nanofibrous membranes decorated with reduced graphene oxide–TiO2 for photocatalytic templates in water purification. *Journal of Materials Science*, *55*(14), 5892–5907. https://doi.org/10.1007/s10853-020-04414-y

Tian, Z., Wang, S., Wu, Y., Yan, F., Qin, S., Yang, J., Li, J., & Cui, Z. (2022). Fabrication of polymer@TiO2 NPs hybrid membrane based on covalent bonding and coordination and its mechanism of enhancing photocatalytic performance. *Journal of Alloys and Compounds*, *910*. https://doi.org/10.1016/j.jallcom.2022.164887

Xu, H., Ding, M., Chen, W., Li, Y., & Wang, K. (2018). Nitrogen–doped GO/TiO2 nanocomposite ultrafiltration membranes for improved photocatalytic performance. *Separation and Purification Technology*, *195*, 70–82. https://doi.org/10.1016/J.SEPPUR.2017.12.003

Yang, G., Zhang, D., Zhu, G., Zhou, T., Song, M., Qu, L., Xiong, K., & Li, H. (2020). A Sm-MOF/GO nanocomposite membrane for efficient organic dye removal from wastewater. *RSC Advances*, *10*(14), 8540–8547. https://doi.org/10.1039/D0RA01110J

Yanilmaz, M., Zhu, J., Lu, Y., Ge, Y., & Zhang, X. (2017). High-strength, thermally stable nylon 6,6 composite nanofiber separators for lithium-ion batteries. *Journal of Materials Science*, *52*(9), 5232–5241. https://doi.org/10.1007/s10853-017-0764-8

Zakaria, N., Rohani, R., Wan Mohtar, W. H. M., Purwadi, R., Sumampouw, G. A., & Indarto, A. (2023). Batik Effluent Treatment and Decolorization—A Review. In *Water (Switzerland)*, 15, (7). https://doi.org/10.3390/w15071339

Zhang, J., Wu, H., Shi, L., Wu, Z., Zhang, S., Wang, S., & Sun, H. (2024). Photocatalysis coupling with membrane technology for sustainable and continuous purification of wastewater. *Separation and*

ISSN: 1410-394X
e-ISSN: 2460-8203

Purification Technology, *329*. https://doi.org/10.1016/j.seppur.2023.125225

Zhang, J., Zheng, M., Zhou, Y., Yang, L., Zhang, Y., Wu, Z., Liu, G., & Zheng, J. (2022). Preparation of Nano-TiO2-Modified PVDF Membranes with Enhanced Antifouling Behaviors via Phase Inversion: Implications of Nanoparticle Dispersion Status in Casting Solutions. *Membranes*, *12*(4). https://doi.org/10.3390/membranes12040386